One-Step Synthesis of Large-Scale Graphene Film Doped with Gold

DATASET · DECEMBER 2014

7 AUTHORS, INCLUDING:

Jingfeng Li
Universität Bremen
24 PUBLICATIONS **209** CITATIONS
SEE PROFILE

Gang Wei
Universität Bremen
81 PUBLICATIONS **1,096** CITATIONS
SEE PROFILE

Zhiqiang Su
Beijing University of Chemical Technology
65 PUBLICATIONS **634** CITATIONS
SEE PROFILE

Langmuir

Article

pubs.acs.org/Langmuir

One-Step Synthesis of Large-Scale Graphene Film Doped with Gold Nanoparticles at Liquid−Air Interface for Electrochemistry and Raman Detection Applications

Panpan Zhang,[†] Ying Huang,[†] Xin Lu,[†] Siyu Zhang,[†] Jingfeng Li,[‡] Gang Wei,*[,‡] and Zhiqiang Su*[,†]

[†]Beijing Key Laboratory on Preparation and Processing of Novel Polymeric Materials, Beijing University of Chemical Technology, 100029, Beijing, China

[‡]Hybrid Materials Interfaces Group, Faculty of Production Engineering, University of Bremen, D-28359 Bremen, Germany

ABSTRACT: We demonstrated a facile one-step synthesis strategy for the preparation of a large-scale reduced graphene oxide multilayered film doped with gold nanoparticles (RGO/AuNP film) and applied this film as functional nanomaterials for electrochemistry and Raman detection applications. The related applications of the fabricated RGO/AuNP film in electrochemical nonenzymatic H_2O_2 biosensor, electrochemical oxygen reduction reaction (ORR), and surface-enhanced Raman scattering (SERS) detection were investigated. Electrochemical data indicate that the H_2O_2 biosensor fabricated by RGO/AuNP film shows a wide linear range, low limitation of detection, high selectivity, and long-term stability. In addition, it was proved that the created RGO/AuNP film also exhibits excellent ORR electrochemical catalysis performance. The created RGO/AuNP film, when serving as SERS biodetection platform, presents outstanding performances in detecting 4-aminothiophenol with an enhancement factor of approximately 5.6×10^5 as well as 2-thiouracil sensing with a low concentration to 1 μM. It is expected that this facile strategy for fabricating large-scale graphene film doped with metallic nanoparticles will spark inspirations in preparing functional nanomaterials and further extend their applications in drug delivery, wastewater purification, and bioenergy.

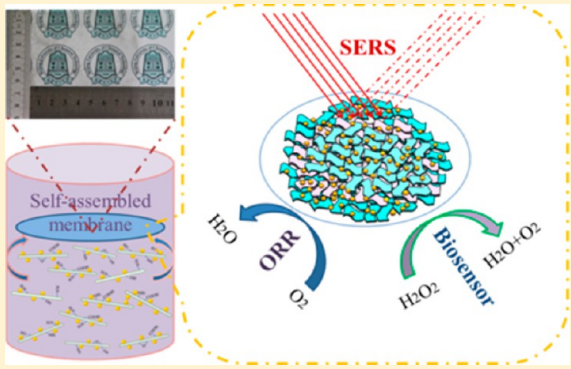

INTRODUCTION

Graphene and its derivatives, as one of the hottest research topics in recent years, have been applied in various fields such as nanoelectronics, energy storage, material science, and biotechnology due to their unique physical and chemical properties.[1,2] Hybridization of graphene or its derivatives with various organic and inorganic nanomaterials has always been a research hotspot recently. These functional hybrid nanomaterials have versatile and tailor-made properties with performances far superior to those of the individual materials.[2−5] It is worth noting that the graphene-based hybrid materials have great significances for biosensing, catalysis, and biodetection.[6−10] Therefore, it is fundamentally important to explore the performances and properties of graphene-based hybrid materials in biological fields.

In order to take full advantage of graphene or its derivatives for biological applications, appropriately functionalization with biomolecules (protein, DNA, peptide, and biopolymer) have been explored previously.[11−14] For biomolecules/graphene hybrids, graphene and its derivatives can provide promising substrates or scaffold for various biological applications due to their large specific surface area and excellent electric conductivity.[2] Biomolecules play important roles in biocompatibility, and the functional groups on the surface of biomolecules can influence the interactions of graphene or its derivatives with cells and tissues. However, due to the defects of degeneration, inactivation, and autolysis of biomolecules, the application of the graphene/biomolecule hybrids is limited.

Recently, various RGO/metal nanoparticle (MNP) hybrids have been synthesized and developed rapidly. The RGO/MNP hybrid nanomaterials have unique optical, chemical, electrical, and catalytic properties and present excellent performance when they are utilized for distinctive bioapplications.[15,16] Among the most popular MNPs, gold nanoparticle (AuNP) is the most stable one. Therefore, it was usually used to functionalize graphene or its derivatives. The RGO/AuNP hybrids present fascinating aspects such as multiple types, size-related electronic, magnetic, and optical properties, and have wide applications in catalytical and biological fields.[17,18]

As special hybrid nanomaterials, graphene-based hybrid films and membranes attracted much attention in the past few years.[19−22] Hybrid films, compared to bulk materials, have advantages of low cost, large area, lightweight, and easy preparation. In addition, the graphene-based hybrid films or membranes are also found to have improved electrical, catalytic, chemical, and mechanical performances. For instance, graphene or its derivative hybrid films, combining with other nanoscale

Received: June 20, 2014
Published: July 11, 2014

   dx.doi.org/10.1021/la5024086 | *Langmuir* 2014, 30, 8980−8989

building blocks such as carbon nanotubes, silica, and platinum nanoparticles, can be used as supercapacitor, conductor, and sensor materials.[19−22] The prepared graphene/AuNP film by doping graphene with AuNPs may achieve their full potentials involving their individual and complex properties.

Herein, we reported a facile one-step green synthesis of a large-scale reduced graphene oxide (RGO) film doped with AuNPs and explored its multibioapplications. Sodium citrate and ammonia were utilized to reduce GO and $HAuCl_4$ in the liquid system simultaneously, and RGO/AuNP film was formed at the liquid−air interface by a self-assembly process. The morphology, structure, and properties of the created RGO/AuNP film were investigated. The aim of our work is to produce the RGO/AuNP film for electrochemical and Raman detection applications. To this end, the prepared RGO/AuNP film was transferred onto glass carbon electrode (GCE) and silicon wafer and further utilized for electrochemistry-based H_2O_2 biosensor and oxygen reduction reaction (ORR) and surface-enhanced Raman scattering (SERS) active substrate for biodetection, respectively. The synthesized film has the advantages of low cost, simple fabrication process, high efficiency, and versatility. We believe that the improved biorelated performances of our graphene film are ascribed to the unique multilayered sandwich-like structure, dense AuNP doping on RGO, and larger surface area to volume ratio. The exploration of electrochemical and SERS applications related to graphene film may be very helpful and important for developing novel nanomaterials with multifunctions.

EXPERIMENTAL SECTION

Reagents and Materials. Natural graphite flake (99.8% purity), chloroauric acid ($HAuCl_4{\cdot}3H_2O$, ≥49.0% Au basis), and sodium citrate tribasic dehydrate (≥99.0% purity) were purchased from Sigma-Aldrich. Ascorbic acid (AA), uric acid (UA), dopamine (DA), 4-aminothiophenol (4-ATP), and 2-thiouracil (2-TU) were obtained from J&K Scientific Ltd. (Beijing, China). H_2O_2 (analytical grade, 30% aqueous solution) was supplied by Tianjin Dongfang Chemical Plant (Tianjin, China). All chemicals used in this work were of analytical reagent grade and obtained from commercial sources and directly used without additional purification. The water used was purified through a Millipore system (~18.2 MΩ·cm). Carbon-coated Cu grids for transmission electron microscopy (TEM) characterization were purchased from Plano GmbH (Wetzlar, Germany).

Synthesis of GO. GO was synthesized by the oxidation of natural graphite flake according to the modifying Hummers method.[23] In detail, 3 g of graphite flakes was mixed with concentrated phosphoric acid (40 mL) and sulfuric acid (360 mL) under stirring at room temperature; then potassium permanganate (18 g) was added slowly, and the mixture was incubated and stirred in the thermostatic water bath for 12 h (50 °C). When the temperature was dropped to room temperature, the mixture was poured slowly onto ice crush (200 mL) and 10% hydrogen peroxide (10 mL). After that, the luminous yellow solution was centrifuged (4000 rpm for 0.5 h), and the supernatant was decanted away. The remaining solid material was then washed in succession with 400 mL of water, 400 mL of 30% hydrochloric acid, and 400 mL of ethanol (2×); for each wash, the supernatant decanted away. The material remaining after multiple-wash process was coagulated with 200 mL of diethyl ether, and the resulting suspension was filtered through a PTFE membrane with a 0.22 μm pore size. The obtained solid on the filter was vacuum-dried overnight at room temperature, and 6.2 g of product was obtained.

Synthesis of AuNPs. AuNPs were synthesized according to the typical sodium citrate reduction method.[24] Briefly, a 100 mL sample of aqueous $HAuCl_4$ (0.01%) in 250 mL flask was brought to boil under punchy stirring. Then 4 mL of aqueous sodium citrate (1%) was added, and the reaction was allowed to run until the solution reached a wine red color, which indicated the reaction was completed.

Fabrication of RGO and RGO/AuNP Films. Aqueous GO (0.5 mg/mL, 100 mL) was sonicated for 2 h and boiled with vigorous stirring. Then 4 mL of aqueous sodium citrate (1.2 g) and ammonia (6 mL) was added successively into the boiled GO solution. The reaction was running for 1 h, and the final black dispersion was incubated at 80 °C for the formation of RGO film. To prepare the RGO/AuNP film, the mixture solution of GO (50 mg, 0.5 mg/mL) and $HAuCl_4$ (300 μL, 507.83 mM) was boiled. After that, 4 mL of aqueous sodium citrate (1.24 g) and ammonia (6.8 mL) were added. The reaction was continued for 1.5 h, and the dark-purple dispersion was dropped to 80 °C for the formation of film.

Fabrication of RGO-, AuNP-, and RGO/AuNP Film-Modified Electrodes. The GCE (3.0 mm in diameter) was polished with 1 and 0.3 μm alumina slurry, then successively washed with ethanol and distilled water in an ultrasonic bath, and finally dried in air. For the preparation of AuNP-modified GCE, 10 μL of the AuNP solution was dropped onto the pretreated GCE and dried in air. The RGO- and RGO/AuNP film-modified GCEs were made by directly transferring the membranes onto the surface of GCEs. The modified electrodes were used for the CV and amperometric response experiments.

H_2O_2 Biosensor. All the electrochemical experiments were carried out using an electrochemical workstation (CHI760D, Chenhua, Shanghai) at room temperature. In the biosensor experiment, a conventional three-electrode system was employed with a modified GCE as working electrode, a Pt wire as auxiliary electrode, and a KCl saturated calomel electrode (SCE) as reference electrode. The test solution was phosphate buffer solutions (PBS, 0.1 M) with pH = 7.6, which were prepared with 0.1 M NaH_2PO_4 and 0.1 M Na_2HPO_4 and deoxygenated with highly pure nitrogen for 20 min before electrochemical experiments. All potentials in this work refer to the SCE. The curves of cyclic voltammograms (CVs) in this work were obtained after six times of scan numbers under steady-state conditions. Amperometric measurements were carried out under stirred conditions.

ORR Catalysis. In the catalysis experiment, a conventional three-electrode system was employed with a modified GCE as working electrode, a Pt wire as auxiliary electrode, and a Ag/AgCl electrode as reference electrode. The test solutions were 0.1 M KOH N_2-saturated solution and O_2-saturated solutions.

SERS Biodetection Platform. In the biodetection experiment, all SERS spectra were recorded using a Renishaw Invia Raman microscope equipped with 10 s integration and 0.1% laser power (785 nm excitation, 250 mW at 100%). The laser beam was positioned through a Leica imaging microscope objective lens (50×), while the instrument's wavenumber was calibrated with a silicon standard centered at 520.5 cm^{-1} shift. Because of the smaller spot size of the laser compared with the large surface area of the samples, the spectra were obtained at three different points of the sample surface. To evaluate the reproducibility and homogeneity of the created RGO/AuNP films for SERS-active substrate, we performed the parallel experiments with three similar samples and tested at least five different points on every sample.

Characterization Techniques. Atomic force microscopy (AFM) images were recorded using a NanoWizard 3 NanoScience atomic force microscope (JPK Instruments AG, Germany) in tapping mode. SEM experiments were performed on JSM-6700F scanning electron microscope (JEOL). The sample surface was deposited on an Au layer to protect the surface layers from ion beam damage. Transmission electron microscopy (TEM) experiments were performed on a Tecnai G220 transmission electron microscope (FEI) with an accelerating voltage of 200 kV, and samples were prepared by transferring the RGO/AuNP film onto the copper grid and dried at room temperature. UV−vis spectroscopy (UV-2900, Hitachi, Japan, scanning rate 400 nm min^{-1}), Fourier transform infrared spectroscopy (FTIR, Nicolet 6700, Thermo-Fisher), X-ray diffraction (XRD, Rigaku D/max-2500 VB +/PC), X-ray photoelectron spectroscopy (XPS, ThermoVG ESCALAB 250), and Raman spectroscopy (LabRAM HORIBA JY,

dx.doi.org/10.1021/la5024086 | Langmuir 2014, 30, 8980−8989

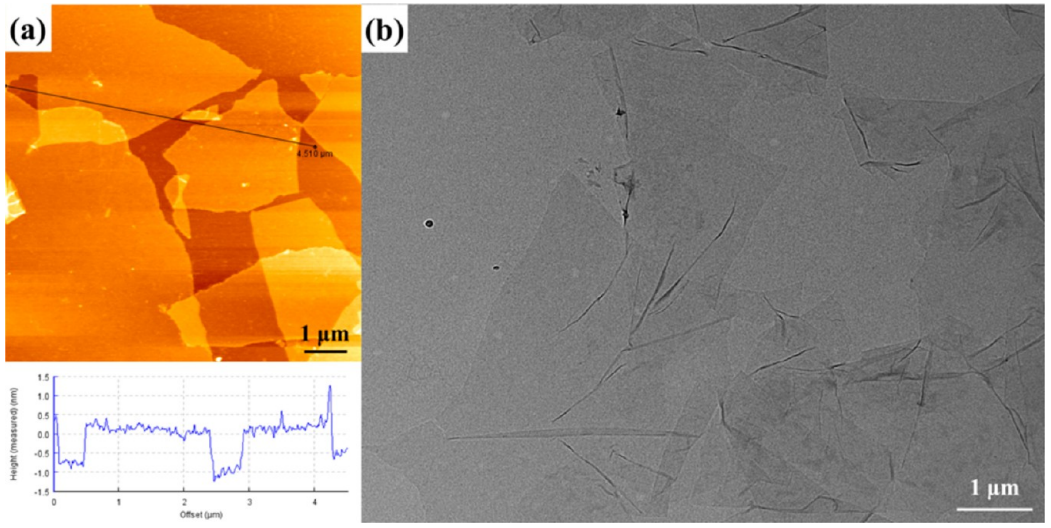

Figure 1. Morphological and structural characterizations of GO: (a) AFM image and section analysis; (b) TEM image.

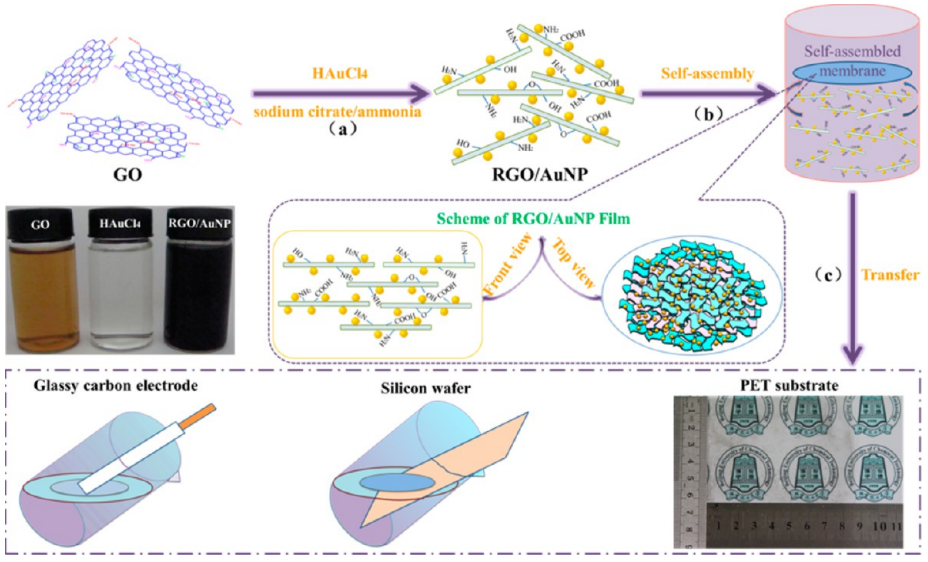

Figure 2. Schematic presentation of the green synthesis and potential formation mechanism of RGO/AuNP film.

Edison, NJ) were used to compare the structures of the GO with RGO/AuNP film.

RESULTS AND DISCUSSION

Characterization of GO. GO was prepared by sonication of graphite oxide, which was synthesized using the modified Hummers method.[23] Figure 1 shows the AFM and TEM images of the single GO nanosheet, which is folded with a height of about 1 nm and a size of about 2 μm. It is known that some reducing agents, such as hydrazine hydrate, sodium borohydride and hydrohalic acids, are toxic and harsh. Therefore, in this work sodium citrate assisted with ammonia as green reducing agent was chosen to prepare RGO, which is also the typical reducing agent for the preparation of AuNPs.[24−26]

Fabrication and Characterizations of RGO/AuNP Film. Graphene-based hybrid films can be obtained via vacuum filtration, spin-coating, spray deposition, and chemical vapor deposition.[27−29] Layer-by-layer (LbL) assembly, directed self-assembly, and electrophoretic deposition have been proved to be useful assembling techniques for fabrication of various nanomaterials.[30−32] In addition, these assembling techniques are simple, facile and eco-friendly for synthesis of novel materials.

Figure 2 shows the schematic green synthesis, self-assembly, and applications of the RGO/AuNP film with a three-stage process. First, GO and $HAuCl_4$ in aqueous solution were mixed together and heated to boiling and simultaneously reduced to RGO and AuNPs by the addition of sodium citrate and ammonia (stage a). Second, the oil bath temperature was decreased to 80 °C for self-assembly into multilayer structure (stage b). The digital pictures of GO, $HAuCl_4$, and RGO/AuNP suspensions are displayed. Finally, a stable and large-scale RGO/AuNP film was harvested from the suspension with a GCE or a silicon wafer for corresponding performance examinations (stage c). The as-prepared RGO/AuNP film on poly(ethylene terephthalate) (PET) substrate is shown in the digital picture (Figure 2), and it is flexible and semitransparent.

We suggest that this formation progress of graphene film has several prominent merits. First, sodium citrate and ammonia as the reducing agents for GO and $HAuCl_4$ are nontoxic and environmentally friendly. Second, the reaction condition is mild

dx.doi.org/10.1021/la5024086 | Langmuir 2014, 30, 8980−8989

and energy-efficient. Third, the simultaneous reduction and self-assembly method are simple and facile.

The morphologies of synthesized AuNPs are shown in Figure 3a,b, and the size of AuNPs is calculated to about 19 nm

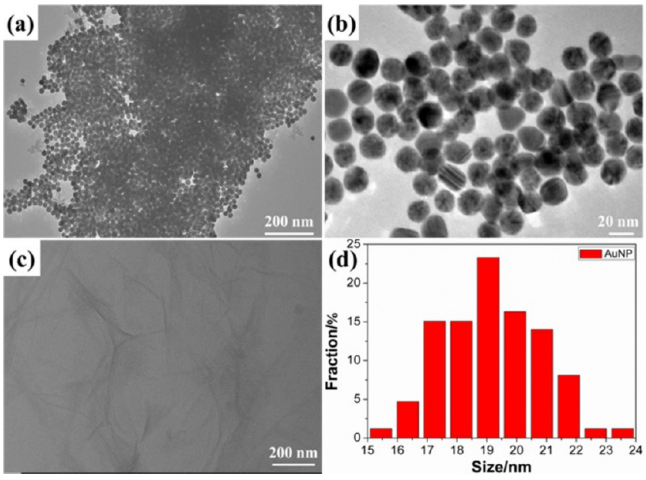

Figure 3. Morphological and structural characterizations of AuNPs and RGO film: (a, b) TEM images of AuNPs with different magnifications, (c) TEM image of self-assembled RGO film, and (d) size distribution of AuNPs.

(Figure 3d). The morphology and structure of the as-prepared RGO/AuNP film were observed by AFM and TEM. Figure 4a,b shows the typical AFM images of the RGO/AuNP film harvested with a silicon substrate. It can be found that some AuNPs are attached onto the surface of the fabricated film. The corresponding AFM section analysis indicates that the height of AuNPs is 4−13 nm, which is consistent with the size

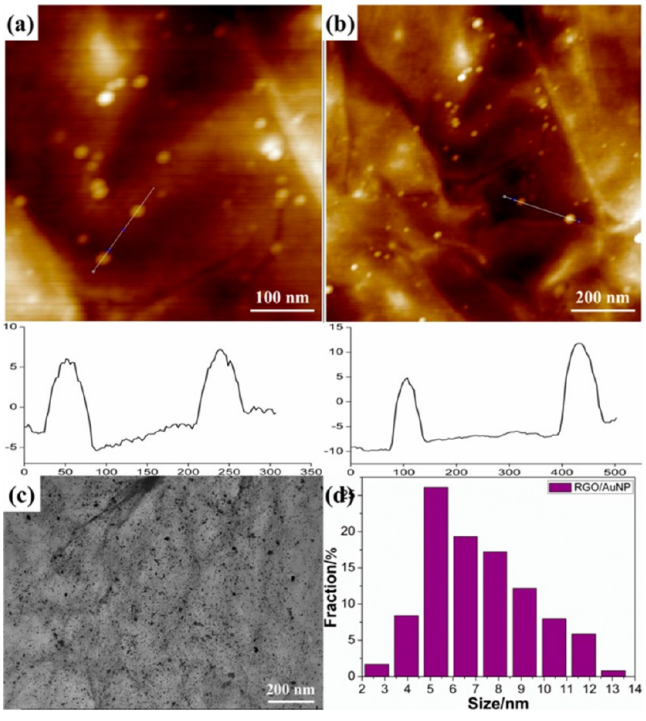

Figure 4. Morphological and structural characterizations of RGO/AuNP film: (a, b) AFM images and section analysis, (c) TEM image, and (d) size distribution of AuNPs in RGO/AuNP film.

distribution image (Figure 4d). It should be noted that, with the help of AFM, only the AuNPs assembled on the surface of film can observed, exclusive of the inner ones between the RGO layers. To observe the internal structure of the sandwich-like multilayer film, RGO/AuNP film was harvested with a copper grid for TEM characterization (Figure 4c). As a control, pure smooth RGO film was prepared with the same method (Figure 3c). As shown in Figure 4c, the RGO/AuNP film is decorated with uniformly dispersed AuNPs. By comparison, it is obvious that more AuNPs are observed in TEM image than that in AFM image, verifying the sandwich-like structure of the created RGO/AuNP film. The thickness of the films fabricated with self-assembly methods has been proved to be controllable and reproducible by adjusting the concentration, temperature, and evaporation period.[33,34]

The large-scale SEM images of RGO/AuNP hybrid film (Figure 5a,b) indicate the unique folded morphology of RGO. In addition, the cross-section analysis could display the multilayer structure obviously, as shown in Figure 5c,d.

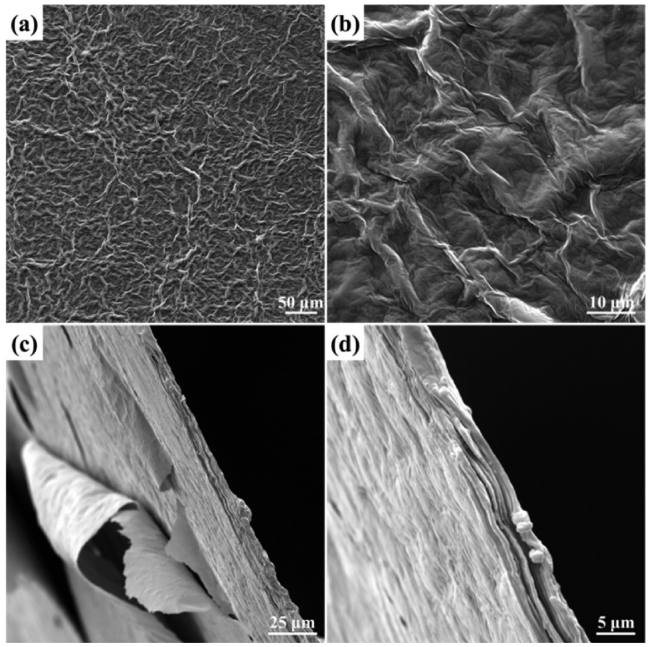

Figure 5. SEM characterization of the created RGO/AuNP films: (a, b) morphology and (c, d) cross-section analysis.

Figure 6 shows the typical TEM images of the RGO/AuNP films with different encapsulations of AuNPs. These samples are prepared by adjusting the dosage of $AuCl_4^-$ ions, and the different dosages are 10, 15, 20, and 25 μL of $HAuCl_4$ (507.83 mM), which are corresponded to the mass ratio of GO to gold salt of 30:1, 20:1, 15:1, and 12:1, respectively. Furthermore, based on the TEM images, the values of the top surface attached AuNPs on each sample are calculated to about 130, 185, 273, and 350 per square micron ($n/\mu m^2$), respectively. It can be observed that the diameter of AuNPs ranges from 4 to 13 nm in all samples. In addition, the density of the AuNPs doping in the RGO/AuNP films increases with the increasing of $HAuCl_4$ concentration for the reduction reaction.

The structural variation of GO before and after reduction was further detected by FT-IR, UV−vis spectroscopy, Raman spectroscopy, XRD, and XPS. Figure 7a shows the FT-IR spectra of GO and RGO/AuNP films. The spectrum of GO

dx.doi.org/10.1021/la5024086 | Langmuir 2014, 30, 8980−8989

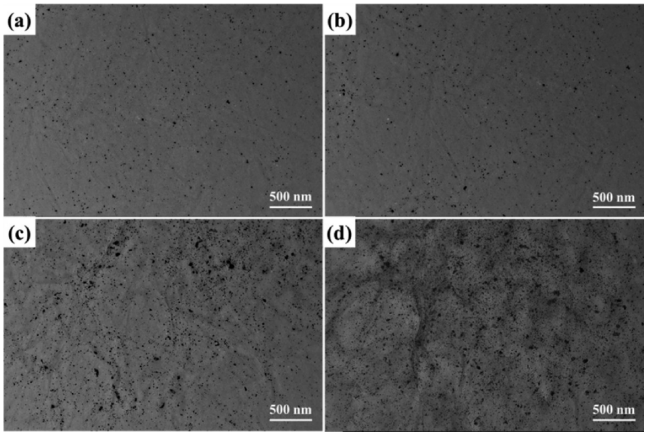

Figure 6. TEM images of RGO/AuNP films with different AuNP encapsulations by adjusting the mass ratio of GO to gold salt to 30:1, 20:1, 15:1, and 12:1.

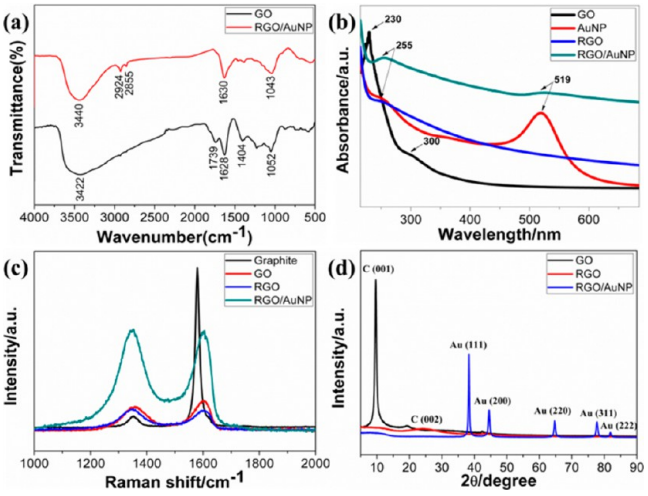

Figure 7. Property and structure characterization of GO, RGO, and RGO/AuNP film: (a) FTIR spectra, (b) UV spectra, (c) Raman spectra, and (d) XRD patterns.

presents several absorption peaks at 3422 and 1404 cm^{-1} (ν_{O-H}), 1739 cm^{-1} (C═O stretching), 1628 cm^{-1} ($\nu_{C=C}$), and 1052 cm^{-1} (ν_{C-O}),[35,36] while after chemical reduction, the characteristic absorption peaks of oxide groups (ν_{O-H}, $\nu_{C=O}$, and ν_{C-O}) in the hybrid film decrease dramatically, indicating that GO has been reduced to the RGO successfully.

The UV−vis absorption spectrum has been proved to be very sensitive to the formation of gold colloids and the structure of graphene-based materials. As shown in Figure 7b, GO exhibits a strong peak centered at 230 nm and a shoulder peak at 300 nm due to the $\pi-\pi^*$ transition of aromatic C═C band and $n-\pi^*$ transition of C═O band, respectively.[10,37] After reduction, the absorption peak at 230 nm red-shifts to 255 nm and the shoulder peak at 300 nm disappears, indicating not only the reduction of GO by sodium citrate and ammonia but also the restoration of the π-conjugation network within RGO. Furthermore, AuNP has a typical strong absorption peak at 519 cm. In the UV−vis absorption spectrum of RGO/AuNP film, both the absorption peaks of RGO and AuNPs can be observed clearly, suggesting the successful reduction of GO and $HAuCl_4$ simultaneously.

The crystalline structure of graphene-based material was detected by Raman spectroscopy. Figure 7c displays the Raman spectra of the RGO/AuNP film and its three related samples. For all the four samples, two peaks at 1350 and 1598 cm^{-1} can be assigned to the D- and G-band, respectively. The D-band is related to the vibration of sp^3 carbon atoms of disordered graphene nanosheets, and the G-band corresponds to vibration of sp^2 carbon atom domains of graphite.[38] The intensity ratios of D- and G-bands (I_D/I_G) of RGO and RGO/AuNP film increased from 0.77 to 1.02 and 1.08, respectively, indicating that most of the oxygenated groups have been removed during the reduction process. Furthermore, the D- and G-bands in RGO and RGO/AuNP film exhibit a small red-shift compared with that of GO, suggesting a potential interaction between RGO and AuNPs.[10] In addition, the intensities of D- and G-bands in RGO/AuNP film are enhanced by ∼500%. This low enhancement factor for RGO/AuNP film indicates the presence of a chemical interaction or bonding between RGO and AuNPs.[39,40] Therefore, we can propose that this RGO is functioned with NH_2, which is prerequisite for the attachment of AuNPs by the N−Au band.

Figure 7d shows the XRD patterns of the prepared GO, RGO, and RGO/AuNP film. The characteristic diffraction peak (001) of GO is observed corresponding to a GO interlayer spacing of ∼9.35 Å, while the peak of RGO shows a dramatic shift to higher 2θ angles with spacing of ∼3.68 Å, indicating that RGO is well-ordered two-dimensional sheets and has smaller average interlayer spacing.[41] In addition, five strong diffraction peaks for RGO/AuNP film are observed, which could be associated with the (111), (200), (220), (311), and (222) planes of the synthesized AuNPs. The diffraction peaks of the synthesized AuNPs are located in the same angles as the Joint Committee on Powder Diffraction Standards (JCPDS), strongly indicating the formation of AuNPs.

Figure 8a presents the XPS spectra of GO, RGO, and RGO/AuNP films. It is established that the bands located at 284.8 and 531.0 eV are associated with the characteristic peaks of C 1s and O 1s, respectively.[42] It is obvious that the O 1s peaks of the RGO and RGO/AuNP film significantly decrease compared to that of GO, verifying the obvious deoxidation effects. In

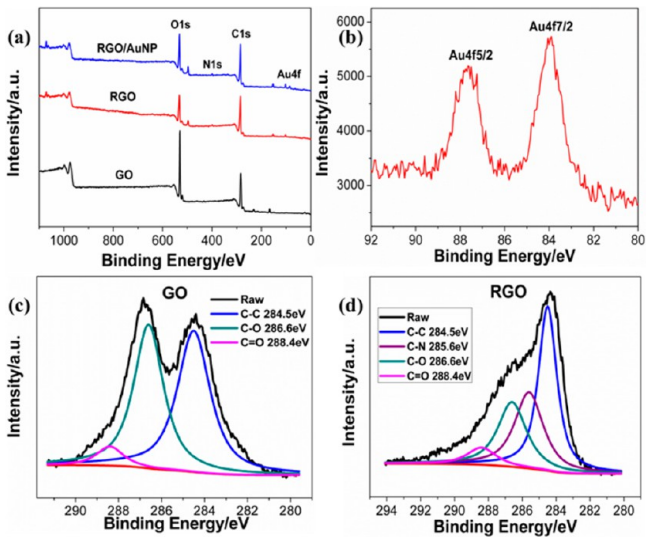

Figure 8. (a, b) XPS spectra of GO, RGO, and RGO/AuNP film; (c, d) C 1s XPS spectra of GO and RGO.

dx.doi.org/10.1021/la5024086 | Langmuir 2014, 30, 8980−8989

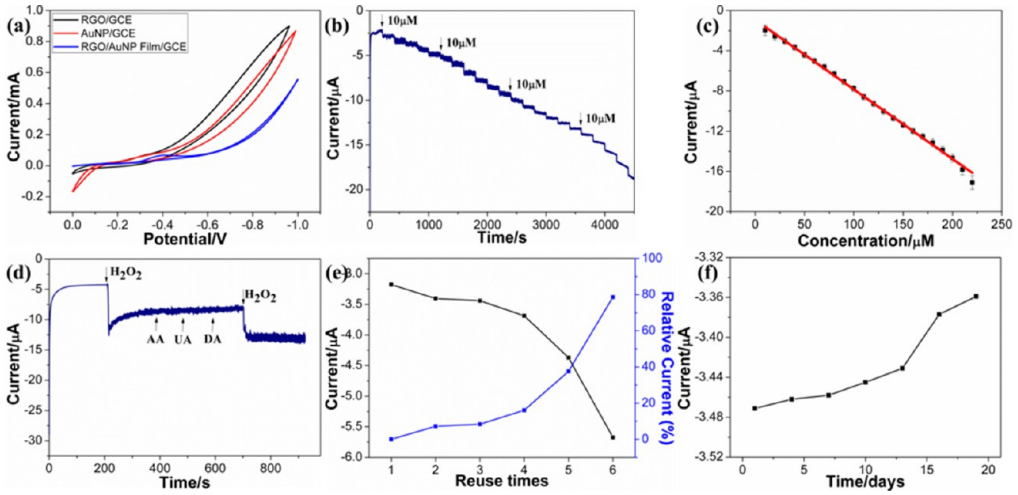

Figure 9. Electrochemical biosensing: (a) CVs of GCEs modified with RGO, AuNP, and RGO/AuNP film. (b) $I-T$ response of the RGO/AuNP film-modified GCE in 0.1 M PBS with successive addition of H_2O_2 at −0.41 V vs SCE. (c) Calibrated line. (d) Selectivity of biosensor. (e) Reusability. (f) Long-term storage stability in response to 40 μM H_2O_2.

addition, a new peak at 400.0 eV associated with N 1s is observed, which can be attributed to the presence of nitrogen element in the ammonia, suggesting the participation of ammonia in the one-step green synthesis.[43] The C 1s peaks of GO and RGO are shown in Figure 8c,d, and it can be disintegrated into four peaks at 284.5 (C−C), 285.6 (C−N), 286.6 (C−O), and 288.4 eV (C═O).[44] The intensity of C−O and C═O peaks of RGO decreases dramatically, and the carbon-to-oxygen atomic ratio of RGO increases from 2.11 to 3.39, indicating the successful chemical reduction progress with sodium citrate and ammonia. Figure 8b displays the Au 4f spectrum, and the peaks shown in 83.8 (Au $4f_{7/2}$) and 87.5 eV (Au $4f_{5/2}$) provide direct evidence for the formation and decoration of AuNPs.[45]

Potential Formation Mechanism of RGO/AuNP Film. Based on the above results, the potential formation mechanism of the RGO/AuNP film was proposed (also see Figure 2). By means of the strong oxidation, the conjugated ring structure of GO has been destructed partially and the oxygen-containing groups have been imported. Following the simultaneous reduction with sodium citrate and ammonia, most of oxygen-containing groups have been removed, and the nitrogen element is successfully introduced onto the surface of RGO. Furthermore, during the formation and growth of AuNPs, RGO sheets have an effect to destroy the nucleation of AuNPs.[46] In the process of simultaneous reduction, the GO and $HAuCl_4$ compete with each other for the same reductant. Under this condition, it is impossible for $HAuCl_4$ to have the homogeneous nucleation to form uniform AuNPs. Therefore, the size of AuNPs in RGO/AuNP film is much smaller than that of pure AuNPs (Figures 3d and 4d), which makes the RGO/AuNP film have excellent performances in biosensing and catalysis. Here we suggest that the simultaneous formed AuNPs have dual interactions with nitrogen-containing RGO, namely physical and chemical interactions. First, AuNPs tend to attach to the defects and residual oxygen-containing groups of RGO sheets under the Brownian motion and electrostatic interaction. Second, after the introduction of N-containing groups, AuNPs can be easily attached onto the RGO sheets by the formation of the N−Au bond. Third, with the continuous evaporation of the mixed solution, there are more opportunities for AuNPs and RGO sheets to interact with each other. When the hybrid suspension was incubated, the solvent evaporation intensified the possibility collision and interaction between free AuNPs and RGO sheets. With the help of Brownian motion, both the RGO and AuNPs can easily move to the liquid−air interface. The surface stress at the liquid−air interface provides a smooth space for the formation of RGO/AuNP film. In addition, the self-assembled film can be easy transferred to other functional materials or modified onto selective substrates, which make it very convenient for some further applications. These factors together determine the formation of multilayer, large-scale, flexile, and semitransparent RGO/AuNP film.

Fabrication of Electrochemical H_2O_2 Biosensor. Combining outstanding electric conductivity of RGO and excellent electrocatalysis property of AuNPs, we expect the created RGO/AuNP film has better performance toward biosensing compared with both RGO and AuNPs. Therefore, the synthesized RGO/AuNP film, as a novel material for fabricating an electrochemical H_2O_2 biosensor, was first investigated in this work. GCEs were polished, sonicated, washed, dried, and covered with RGO, AuNPs, and RGO/AuNP film, respectively, for the subsequent H_2O_2 catalysis and biosensing.

Figure 9a shows the typical CVs of RGO-, AuNP-, and RGO/AuNP film-modified GCEs in the presence of 40 μM H_2O_2. The RGO-modified GCE shows no apparent redox processes, and the AuNP-modified GCE shows a very small current response and a broad reduction peak from about −0.5 to −0.2 V. It is clear that the RGO/AuNP film-modified GCE shows a reduction peak at about −0.41 V and an obvious positive shift of both the onset potential and current peak compared to RGO- and AuNP-modified GCEs. Here we selected −0.41 V as the applied potential for $I-T$ measurements, and a stable response rapidly increased in the cathodic current as a result of the reduction of H_2O_2 upon the addition of H_2O_2 solution (Figure 9b). The calibration curve (Figure 9c) indicates a linear response to H_2O_2; the linear range of the H_2O_2 detection is from 10 to 200 μM (R = 0.9981, S/N = 3), and the limit of detection (LOD) is calculated to be 1.7 μM (S/N = 3) with a sensitivity of 97.8 μA mM^{-1} cm^{-2}. In our previous work, we fabricated a film material of carbon nanotubes and silver nanoparticles by electrospinning, and utilized this film material for biosensor of H_2O_2.[21,22] We found

dx.doi.org/10.1021/la5024086 | Langmuir 2014, 30, 8980−8989

that the self-assembled RGO/AuNP film has better performance (about 10-fold increase) as H_2O_2 biosensor material than that with electrospun film.[47]

The selectivity test is demonstrated in Figure 9d, which compares the amperometric response for three relevant electroactive species, such as ascorbic acid (AA), uric acid (UA), and dopamine (DA) with consistent concentration of 40 μM. No responding was observed at the potential of −0.41 V, indicating the high selectivity toward the detection of H_2O_2. The reuse stability of RGO/AuNP film-modified GCE was also examined (Figure 9e), and the result shows that the repeated usage of the created biosensor is possible for at least five times. Significant reduction in current after five times of use is displayed, which is ascribed to the detachment of the graphene film from the electrode. Finally, the long-term stability of the RGO/AuNP film modified GCE was explored over a 15 day period (Figure 9f). The prepared electrode was stored in a refrigerator at 4 °C and measured every 2−4 days. The result shows that the catalytic current response retains more than 96.8% of its initial value in response to 40 μM H_2O_2 after 15 days, indicating an acceptable stability of the modified electrode.

Fabrication of Cathodic Catalyst for Electrochemical ORR. Oxygen is the most sustainable electron acceptor currently available for the microbial fuel cell cathodes (MFC). In a MFC, bacteria was used an anode as electron acceptor for the oxidation of organic carbon to carbon dioxide and produced protons and electrons.[48] The cathodic ORR is an important process in the biofuel cells and metal−air batteries.[48,49] Not only Pt but also some other noble metals, such as Au, Fe, Ni, and Co, have been explored as an attractive ORR catalyst.[50,51] To maximize the electrocatalytic activity of the ORR catalyst, graphene and its derivatives are utilized as a support to disperse the catalyst as well as to accelerate the migration rate of electrons. Therefore, our RGO/AuNP film may be utilized as a novel kind of electrocatalyst for the ORR with good performance.

Figure 10a shows the CVs of the fabricated RGO/AuNP film-modified GCE in N_2- and O_2-saturated 0.1 M KOH

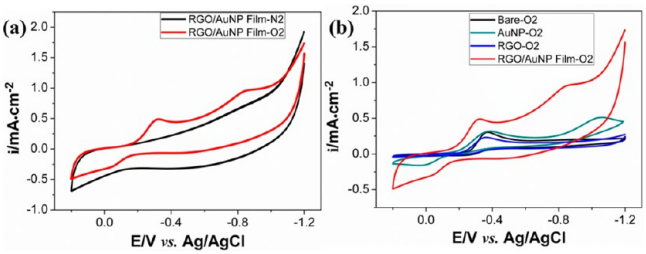

Figure 10. Electrochemical catalysis of ORR with CVs: (a) RGO/AuNP film/GCE in 0.1 M N_2- and O_2-saturated KOH solution, respectively; (b) the same of a bare GCE, AuNPs/GCE, RGO/GCE, and RGO/AuNP film/GCE in 0.1 M O_2-saturated KOH solution at a scan rate of 50 mV/s.

solution, respectively. The peak exhibits only a high capacitive current in the N_2-saturated solution, while a well-defined peak is present at −0.31 V in the O_2-saturated solution. In order to detect the catalysis property of the film, the CVs of a bare GCE, RGO-, AuNP-, and RGO/AuNP film-modified GCEs in O_2-saturated 0.1 M KOH solution are presented in Figure 10b. For the bare GCE, AuNP-, and RGO-modified GCEs, the electrochemical reduction starts at −0.40, −0.28, and −0.19 V, respectively. However, the RGO/AuNP film-modified GCE exhibits more positive onset potential (−0.14 V) and much larger reduction current for the ORR. This result greatly demonstrates the superior electrochemical ORR activity of the created RGO/AuNP film. We suggest that the improved ORR activity is related to the special nanostructure of the created RGO/AuNP film. The loosely sandwich-like and stacking structures may maintain very high specific surface area, and the basic building blocks (AuNPs and RGO nanosheets) can provide enough active reaction sites, which activate the adsorption of O_2 on the surface of graphene film and promote the ORR process efficiently.[52]

Fabrication of SERS Biodetection Platform. SERS as a specific technique for ultrasensitive detection has attracted significant attention. As for the SERS mechanism, it is considered that electromagnetic (EM) and chemical (CM) enhancements coexist.[53] In SERS applications, MNPs (Ag and Au, specially) were greatly employed due to their ability to enhance the local EM field. Furthermore, graphene and its derivatives have also been applied in SERS for the charge transfer occurring between graphene and adsorbed molecules.[53−55] Therefore, graphene−MNPs hybrids can result in a superior Raman enhanced effect due to the coupled EM and CM actions.

Here, we explored the potential of the created RGO/AuNP film as a SERS biodetection platform. In order to confirm the high SERS activity of RGO/AuNP film for the application in SERS-active substrates, 4-aminothiophenol (4-ATP) was chosen as the probe molecule and four different substrates were dipped into 4-ATP ethanol solution with different concentrations for 1 h. After that, the samples were washed, dried, and analyzed by Raman spectroscopy. For comparison, AuNP-, RGO-, and RGO/AuNP film-coated silicon substrates were prepared under the same conditions and used as the SERS-active platforms of 4-ATP molecules (Figure 11a). The results show that no apparent Raman peaks of 4-ATP are detected at RGO platform except D- and G-bonds of RGO. Several strong peaks at 1587 (ν_{C-C}), 1077 (ν_{C-S}), and 387

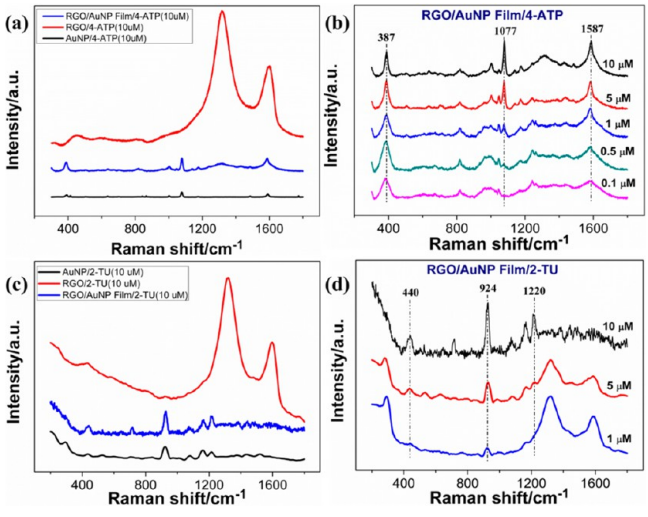

Figure 11. SERS biodetection platform with RGO/AuNP film: (a, c) SERS spectra of (a) 4-ATP and (c) 2-TU with a concentration of 10 μM on AuNPs, RGO, and RGO/AuNP film; (b, d) SERS spectra of (b) 4-ATP (10, 5, 1, 0.5, and 0.1 μM) and (d) 2-TU (10, 5, and 1 μM) on the fabricated RGO/AuNP film.

dx.doi.org/10.1021/la5024086 | Langmuir 2014, 30, 8980−8989

cm^{-1} (ν_{C-H}) are observed in the Raman spectra of AuNPs and RGO/AuNP film, which are assigned to a_1 vibrational modes (in-plane and in-phase modes) of the 4-ATP molecule.[56] To evaluate the potential applications of the RGO/AuNP film for the high-sensitive determination of 4-ATP, these samples were immersed into 4-ATP solutions with different concentrations, and the corresponding SERS spectra are shown in Figure 11b. It can be seen that the Raman intensities increase with the continuous addition of 4-ATP, and 4-ATP solution with very low concentration (as low as 0.1 μM) can be easily detected on this RGO/AuNP film platform. The enhancement factor (EF) of the RGO/AuNP film for detecting 4-ATP can be calculated according to a previous report:[57]

$$\mathrm{EF} = \frac{I_{\mathrm{SERS}}}{I_{\mathrm{bulk}}} \times \frac{M_{\mathrm{bulk}}}{M_{\mathrm{ads}}}$$

where I_{SERS} is the intensity of a specific band in the SERS spectrum of 4-ATP and I_{bulk} is the intensity of the same band in the Raman spectrum from the bulk solution sample. For all spectra, the intensity of the band at 1077 cm^{-1} is used to calculate EF values. M_{bulk} is the number of molecules of the bulk 4-ATP in the laser illumination volume, while M_{ads} is the number of molecules adsorbed and sampled on the SERS active substrate within the laser spot. The RGO/AuNP film, as the SERS substrate for 4-ATP detection, has an EF of 5.6×10^5, which was calculated with the vibration intensity at 1077 cm^{-1}.

Furthermore, the biodetection of 2-thiouracil (2-TU) with the created RGO/AuNP film platforms was also performed. 2-TU is a kind of thio derivative of uracil which belongs to the nucleic acid bases. 2-TU and its derivatives present high antithyroid, antiviral, and antitumor activity according to previous studies,[58,59] and therefore sensitive detection of 2-TU at low concentration is of great importance for the analytical and medical applications. Figure 11c shows the typical SERS spectra of 2-TU (10 μM) on AuNP-, RGO-, and RGO/AuNP film-coated silicon substrates. It is clear that the AuNP- and RGO/AuNP film-coated silicon substrates have obvious signal enhancement for the detection of 2-TU molecules. The overall spectral features for both samples are agreed well with that presented in the previous reports.[24,27] Two characteristic SERS peaks of 2-TU at 924 and 1220 cm^{-1} can be found. The significant enhancement in the intensity of peak at 924 cm^{-1} is ascribed to the plane bending of N(3)CC and rings, and the nonprominent enhancement at 1220 cm^{-1} is corresponding to the in-plane bending of C(5)−H and C(6)−H.[59] It should be noted that the RGO also has a very weak enhancement for the intensity of peak at 924 cm^{-1}, and therefore we suggest that RGO film can enhance the Raman signals of 2-TU due to the noncovalent interaction between RGO and 2-TU molecules. Figure 11d shows the typical SERS spectra of 2-TU with different concentrations (1-10 μM) on the RGO/AuNP film-coated silicon substrate. The obtained result indicates that, with the help of RGO/AuNP film platform, 2-TU with a low concentration (approximately 1 μM) can be effective detected. Based on the SERS detection results of 4-ATP and 2-TU molecules, the potential application of the RGO/AuNP film as biodetection platform is confirmed.

CONCLUSION

In summary, for the first time we prepared a sandwich-like multilayered RGO/AuNP film with a facile green synthesis and self-assembly method. Under the influence of the N−Au bond, Brownian motion, and electrostatic interaction, the simultaneous reduced AuNPs have smaller size and uniformly disperse on the surface of RGO, which endows the fabricated RGO/AuNP film superior performances in electrochemical biosensor and catalysis as well as SERS detection. Compared to previous methods, our strategy for producing RGO-based composite film has several advantages, such as environmental friendliness, time saving, high efficiency, and cost-effectiveness. In addition, the created RGO/AuNP hybrid film can be transferred directly onto GCEs or silicon wafers for electrochemical and SERS applications without further complex postprocess. The novelty and significance of this RGO/AuNP film can be reflected in excellent performances for its enhanced biorelated applications including H_2O_2 biosensor, ORR catalysis, and SERS detection. It is expected that this green synthesis method can be utilized to prepare other multifunctional film materials based on graphene and nanoparticles and extend the potential applications in biomaterials, biomedicine science, electrochemistry, and analytical science.

AUTHOR INFORMATION

Corresponding Authors

*E-mail wei@uni-bremen.de (G. Wei).

*E-mail suzq@mail.buct.edu.cn (Z.Q. Su).

Notes

The authors declare no competing financial interest.

ACKNOWLEDGMENTS

The authors gratefully acknowledge the financial support from the Fundamental Research Funds for the Central Universities (project no. ZZ1307). We thank the financial support of the China Scholarship Council (CSC) for PhD scholarships.

REFERENCES

(1) Georgakilas, V.; Otyepka, M.; Bourlinos, A. B.; Chandra, V.; Kim, N.; Kemp, K. C.; Hobza, P.; Zboril, R.; Kim, K. S. Functionalization of graphene: covalent and non-covalent approaches, derivatives and applications. *Chem. Rev.* **2012**, *112*, 6156−6214.

(2) Guo, S.; Dong, S. Graphene nanosheet: synthesis, molecular engineering, thin film, hybrids, and energy and analytical applications. *Chem. Soc. Rev.* **2011**, *40*, 2644−2672.

(3) Quintana, M.; Vazquez, E.; Prato, M. Organic functionalization of graphene in dispersions. *Acc. Chem. Res.* **2013**, *46*, 138−148.

(4) Bai, S.; Shen, X. Graphene-inorganic nanocomposites. *RSC Adv.* **2012**, *2*, 64−98.

(5) Kamat, P. V. Graphene-based nanoarchitectures. anchoring semiconductor and metal nanoparticles on a two-dimensional carbon support. *J. Phys. Chem. Lett.* **2010**, *1*, 520−527.

(6) Wang, Y.; Li, Z.; Wang, J.; Li, J.; Lin, Y. Graphene and graphene oxide: biofunctionalization and applications in biotechnology. *Trends Biotechnol.* **2011**, *29*, 205−212.

(7) Zhu, Y.; Murali, S.; Cai, W.; Li, X.; Suk, J. W.; Potts, J. R.; Ruoff, R. S. Graphene and graphene oxide: synthesis, properties, and applications. *Adv. Mater.* **2010**, *22*, 3906−3924.

(8) Fang, Y.; Guo, S.; Zhu, C.; Zhai, Y.; Wang, E. Self-assembly of cationic polyelectrolyte-functionalized graphene nanosheets and gold nanoparticles: a two-dimensional heterostructure for hydrogen peroxide sensing. *Langmuir* **2010**, *26*, 11277−11282.

(9) Mao, S.; Lu, G.; Yu, K.; Bo, Z.; Chen, J. Specific protein detection using thermally reduced graphene oxide sheet decorated with gold nanoparticle-antibody conjugates. *Adv. Mater.* **2010**, *22*, 3521−3526.

(10) Lv, X.; Weng, J. Ternary composite of hemin, gold nanoparticles and graphene for highly efficient decomposition of hydrogen peroxide. *Sci. Rep.* **2013**, *3*, 3285.

(11) Guo, C. X.; Zheng, X. T.; Lu, Z. S.; Lou, X. W.; Li, C. M. Biointerface by cell growth on layered graphene-artificial peroxidase-protein nanostructure for in situ quantitative molecular detection. *Adv. Mater.* **2010**, *22*, 5164−5167.
(12) Patil, A. J.; Vickery, J. L.; Scott, T. B.; Mann, S. Aqueous stabilization and self-assembly of graphene sheets into layered bio-nanocomposites using DNA. *Adv. Mater.* **2009**, *21*, 3159−3164.
(13) Wang, H.; Zhang, Q.; Chu, X.; Chen, T.; Ge, J.; Yu, R. Graphene oxide-peptide conjugate as an intracellular protease sensor for caspase-3 activation imaging in live cells. *Angew. Chem., Int. Ed.* **2011**, *50*, 7065−7069.
(14) Cheng, C.; Nie, S.; Li, S.; Peng, H.; Yang, H.; Ma, L.; Sun, S.; Zhao, C. Biopolymer functionalized reduced graphene oxide with enhanced biocompatibility via mussel inspired coatings/anchors. *J. Mater. Chem. B* **2013**, *1*, 265−275.
(15) Rosi, N. L.; Mirkin, C. A. Nanostructures in biodiagnostics. *Chem. Rev.* **2005**, *105*, 1547−1562.
(16) Tan, C.; Huang, X.; Zhang, H. Synthesis and applications of graphene-based noble metal nanostructures. *Mater. Today* **2013**, *16*, 29−36.
(17) Daniel, M. C.; Astruc, D. Gold nanoparticles: assembly, supramolecular chemistry, quantum-size-related properties, and applications toward biology, catalysis, and nanotechnology. *Chem. Rev.* **2004**, *104*, 293−346.
(18) Huang, J.; Zhang, L.; Chen, B.; Ji, N.; Chen, F.; Zhang, Y.; Zhang, Z. Nanocomposites of size-controlled gold nanoparticles and graphene oxide: formation and applications in SERS and catalysis. *Nanoscale* **2010**, *2*, 2733−2738.
(19) Yu, D.; Dai, L. Self-assembled graphene/carbon nanotube hybrid films for supercapacitors. *J. Phys. Chem. Lett.* **2010**, *1*, 467−470.
(20) Watcharotone, S.; Dikin, D. A.; Stankovich, S.; Piner, R.; Jung, I.; Dommett, G. H. B.; Evmenenko, G.; Wu, S. E.; Chen, S. F.; Liu, C. P.; Nguyen, S. T.; Ruoff, R. S. Graphene-silica composite thin films as transparent conductors. *Nano Lett.* **2007**, *7*, 1888−1892.
(21) Ouyang, Z.; Li, J.; Wang, J.; Li, Q.; Ni, T.; Zhang, X.; Wang, H.; Li, Q.; Su, Z.; Wei, G. Fabrication, characterization and sensor application of electrospun polyurethane nanofibers filled with carbon nanotubes and silver nanoparticles. *J. Mater. Chem. B* **2013**, *1*, 2415−2424.
(22) Zhang, P.; Zhao, X.; Zhang, X.; Lai, Y.; Wang, X.; Li, J.; Wei, G.; Su, Z. Electrospun doping of carbon nanotubes and platinum nanoparticles into the β-phase polyvinylidene difluoride nanofibrous membrane for biosensor and catalysis applications. *ACS Appl. Mater. Interfaces* **2014**, *6*, 7563−7571.
(23) Marcano, D. C.; Kosynkin, D. V.; Berlin, J. M.; Sinitskii, A.; Sun, Z.; Slesarev, A.; Alemany, L. B.; Lu, W.; Tour, J. M. Improved synthesis of graphene oxide. *ACS Nano* **2010**, *4*, 4806−4814.
(24) Ji, X.; Song, X.; Li, J.; Bai, Y.; Yang, W.; Peng, X. Size control of gold nanocrystals in citrate reduction: the third role of citrate. *J. Am. Chem. Soc.* **2007**, *129*, 13939−13948.
(25) Zhou, X.; Huang, X.; Qi, X.; Wu, S.; Xue, C.; Boey, F. Y. C.; Yan, Q.; Chen, P.; Zhang, H. In situ synthesis of metal nanoparticles on single-layer graphene oxide and reduced graphene oxide surfaces. *J. Phys. Chem. C* **2009**, *113*, 10842−10846.
(26) Zhang, Z.; Chen, H.; Xing, C.; Guo, M.; Xu, F.; Wang, X.; Gruber, H. J.; Zhang, B.; Tang, J. Sodium citrate: a universal reducing agent for reduction/decoration of graphene oxide with Au nanoparticles. *Nano Res.* **2011**, *4*, 599−611.
(27) Kim, H. W.; Yoon, H. W.; Yoon, S. M.; Yoo, B. M.; Ahn, B. K.; Cho, Y. H.; Shin, H. J.; Yang, H.; Paik, U.; Kwon, S.; Choi, J. Y.; Park, H. B. Selective gas transport through few-layered graphene and graphene oxide membranes. *Science* **2013**, *342*, 91−95.
(28) Mulpur, P.; Podila, R.; Lingam, K.; Vemula, S. K.; Ramamurthy, S. S.; Kamisetti, V.; Rao, A. M. Amplification of surface plasmon coupled emission from graphene-Ag hybrid films. *J. Phys. Chem. C* **2013**, *117*, 17205−17210.
(29) Li, X.; Zhao, T.; Wang, K.; Yang, Y.; Wei, J.; Kang, F.; Wu, D.; Zhu, H. Directly drawing self-assembled, porous, and monolithic graphene fiber from chemical vapor deposition grown graphene film and its electrochemical properties. *Langmuir* **2011**, *27*, 12164−12171.
(30) Kong, B. S.; Geng, J.; Jung, H. T. Layer-by-layer assembly of graphene and gold nanoparticles by vacuum filtration and spontaneous reduction of gold ions. *Chem. Commun.* **2009**, 2174−2176.
(31) Xi, Q.; Chen, X.; Evans, D. G.; Yang, W. Gold nanoparticle-embedded porous graphene thin films fabricated via layer-by-layer self-assembly and subsequent thermal annealing for electrochemical sensing. *Langmuir* **2012**, *28*, 9885−9892.
(32) Wu, Z. S.; Pei, S.; Ren, W.; Tang, D.; Gao, L.; Liu, B.; Li, F.; Liu, C.; Cheng, H. M. Field emission of single-layer graphene films prepared by electrophoretic deposition. *Adv. Mater.* **2009**, *21*, 1756−1760.
(33) Chen, C.; Yang, Q. H.; Yang, Y.; Lv, W.; Wen, Y.; Hou, P. X.; Wang, M.; Cheng, H. M. Self-assembled free-standing graphite oxide membrane. *Adv. Mater.* **2009**, *21*, 3007−3011.
(34) Sun, S.; Wu, P. Easy fabrication of macroporous gold films using graphene sheets as a template. *ACS Appl. Mater. Interfaces* **2013**, *5*, 3481−3486.
(35) Moon, I. K.; Lee, J.; Ruoff, R. S.; Lee, H. Reduced graphene oxide by chemical graphitization. *Nat. Commun.* **2010**, *1*, 73.
(36) Huang, K. J.; Niu, D. J.; Liu, X.; Wu, Z. W.; Fan, Y.; Chang, Y. F.; Wu, Y. Y. Direct electrochemistry of catalase at amine-functionalized graphene/gold nanoparticles composite film for hydrogen peroxide sensor. *Electrochim. Acta* **2011**, *56*, 2947−2953.
(37) Li, D.; Müller, M. B.; Gilje, S.; Kaner, R. B.; Wallace, G. G. Processable aqueous dispersions of graphene nanosheets. *Nat. Nanotechnol.* **2008**, *3*, 101−105.
(38) Gao, J.; Liu, F.; Liu, Y.; Ma, N.; Wang, Z.; Zhang, X. Environment-friendly method to produce graphene that employs vitamin C and amino acid. *Chem. Mater.* **2010**, *22*, 2213−2218.
(39) Jasuja, K.; Berry, V. Implantation and growth of dendritic gold nanostructures on graphene derivatives: electrical property tailoring and Raman enhancement. *ACS Nano* **2009**, *3*, 2358−2366.
(40) Campion, A.; Ivanecky, J. E.; Child, C. M.; Foster, M. On the mechanism of chemical enhancement in surface-enhanced Raman-scattering. *J. Am. Chem. Soc.* **1995**, *117*, 11807−11808.
(41) Zhu, C.; Guo, S.; Fang, Y.; Dong, S. Reducing sugar: new functional molecules for the green synthesis of graphene nanosheets. *ACS Nano* **2010**, *4*, 2429−2437.
(42) Park, S.; An, J.; Piner, R. D.; Jung, I.; Yang, D.; Velamakanni, A.; Nguyen, S. T.; Ruoff, R. S. Aqueous suspension and characterization of chemically modified graphene sheets. *Chem. Mater.* **2008**, *20*, 6592−6594.
(43) Li, X.; Wang, H.; Robinson, J. T.; Sanchez, H.; Diankov, G.; Dai, H. Simultaneous nitrogen-doping and reduction of graphene oxide. *J. Am. Chem. Soc.* **2009**, *131*, 15939−15944.
(44) Liu, S.; Tian, J.; Wang, L.; Sun, X. A method for the production of reduced graphene oxide using benzylamine as a reducing and stabilizing agent and its subsequent decoration with Ag nanoparticles for enzymeless hydrogen peroxide detection. *Carbon* **2011**, *49*, 3158−3164.
(45) Wei, G.; Pan, C.; Reichert, J.; Jandt, K. D. Controlled assembly of protein-protected gold nanoparticles on noncovalent functionalized carbon nanotubes. *Carbon* **2010**, *48*, 645−653.
(46) Tien, H. W.; Huang, Y. L.; Yang, S. Y.; Wang, J. Y.; Ma, C. C. M. The production of graphene nanosheets decorated with silver nanoparticles for use in transparent, conductive films. *Carbon* **2011**, *49*, 1550−1560.
(47) Hong, W.; Bai, H.; Xu, Y.; Yao, Z.; Gu, Z.; Shi, G. Preparation of gold nanoparticle/graphene composites with controlled weight contents and their application in biosensors. *J. Phys. Chem. C* **2010**, *114*, 1822−1826.
(48) Freguia, S.; Rabaey, K.; Yuang, Z.; Keller, J. Non-catalyzed cathodic oxyagen reduction at graphite granules in microbial fuel cell. *Electrochim. Acta* **2007**, *53*, 598−603.
(49) Stamenkovic, V. R.; Fowler, B.; Mun, B. S.; Wang, G.; Ross, P. N.; Lucas, C. A.; Markovic, N. M. Improved oxygen reduction activity

on $Pt_3Ni(111)$ via increased surface site availability. *Science* **2007**, *315*, 493−497.
(50) Wang, C.; Vliet, D.; More, K. L.; Zaluzec, N. J.; Peng, S.; Sun, S.; Daimon, H.; Wang, G.; Greeley, J.; Pearson, J.; Paulikas, A. P.; Karapetrov, G.; Strmcnik, D.; Markovic, N. M.; Stamenkovic, V. R. Multimetallic Au/$FePt_3$ nanoparticles as highly durable electrocatalyst. *Nano Lett.* **2011**, *11*, 919−926.
(51) Zhu, C.; Guo, S.; Zhai, Y.; Dong, S. Layer-by-layer self-assembly for constructing a graphene/platinum nanoparticle three-dimensional hybrid nanostructure using ionic liquid as a linker. *Langmuir* **2010**, *26*, 7614−7618.
(52) Wang, F. B.; Wang, J.; Shao, L.; Zhao, Y.; Xia, X. H. Hybrids of gold nanoparticles highly dispersed on graphene for the oxygen reduction reaction. *Electrochem. Commun.* **2014**, *38*, 82−85.
(53) Lee, J.; Shim, S.; Kim, B.; Shin, H. S. Surface-enhanced Raman scattering of single- and few-layer graphene by the deposition of gold nanoparticles. *Chem. Eur. J.* **2011**, *17*, 2381−2387.
(54) Iliut, M.; Leordean, C.; Canpean, V.; Teodorescu, C. M.; Astilean, S. A new green, ascorbic acid-assisted method for versatile synthesis of Au-graphene hybrids as efficient surface-enhanced Raman scattering platforms. *J. Mater. Chem. C* **2013**, *1*, 4094−4104.
(55) Ling, X.; Xie, L.; Fang, Y.; Xu, H.; Zhang, H.; Kong, J.; Dresselhaus, M. S.; Zhang, J.; Liu, Z. Can graphene be used as a substrate for Raman enhancement? *Nano Lett.* **2010**, *10*, 553−561.
(56) Wei, G.; Wang, L.; Sun, L.; Song, Y.; Sun, Y.; Guo, C.; Yang, T.; Li, Z. Type I collagen-mediated synthesis and assembly of UV-photoreduced gold nanoparticles and their application in surface-enhanced Raman scattering. *J. Phys. Chem. C* **2007**, *111*, 1976−1982.
(57) Ngo, Y. H.; Li, D.; Simon, G. P.; Garnier, G. Gold nanoparticle-paper as a three-dimensional surface enhanced Raman scattering substrate. *Langmuir* **2012**, *28*, 8782−8790.
(58) Jena, B. K.; Raj, C. R. Seedless, surfactantless room temperature synthesis of single crystalline fluorescent gold nanoflowers with pronounced SERS and electrocatalytic activity. *Chem. Mater.* **2008**, *20*, 3546−3548.
(59) Aguiar, H. B.; Sant'Ana, A. C.; Temperini, M. L. A.; Corio, P.; Cunha, F. Surface enhanced Raman spectroscopy analysis of the adsorption of 2-thiouracil to Au, Ag and Cu electrodes: surface potential dependence. *Vib. Spectrosc.* **2006**, *40*, 127−132.